Available online at www.sciencedirect.com
ScienceDirect
Journal of Computational Physics 227 (2008) 4873–4894
JOURNAL OF COMPUTATIONAL PHYSICS
www.elsevier.com/locate/jcp

An improved reconstruction method for compressible flows with low Mach number features ☆

B. Thornber [a], A. Mosedale [a], D. Drikakis [a,*], D. Youngs [b], R.J.R. Williams [b]

[a] *Fluid Mechanics and Computational Science Group, Aerospace Sciences Department, School of Engineering, Cranfield University, Cranfield MK43 0AL, United Kingdom*
[b] *AWE, Aldermaston, United Kingdom*

Received 25 April 2007; received in revised form 26 December 2007; accepted 14 January 2008
Available online 2 February 2008

Abstract

This paper proposes a simple modification of the variable reconstruction process within finite volume schemes to allow significantly improved resolution of low Mach number perturbations for use in mixed compressible/incompressible flows. The main advantage is that the numerical method locally adapts the variable reconstruction to allow minimum dissipation of low Mach number features whilst maintaining shock capturing ability, all without modifying the formulation of the governing equations. In addition, incompressible scaling of the pressure and density variations are recovered. Numerical tests using a Godunov-type method demonstrate that the new scheme captures shock waves well, significantly improves resolution of low Mach number features and greatly reduces high wave number dissipation in the case of homogeneous decaying turbulence and Richtmyer–Meshkov mixing. In the latter case, the turbulent spectra match theoretical predictions excellently. Additional computational expense due to the proposed modification is negligible.
© 2008 Elsevier Inc. All rights reserved.

Keywords: Compressible fluid dynamics; Turbulent mixing; Godunov schemes; Dissipation; Kinetic energy; Richtmyer–Meshkov instability; Homogeneous decaying turbulence; Large eddy simulation; Low Mach number features

1. Introduction

Increasing computational power and improvements in numerical methods has meant that simulations of compressible flow configurations are now at such high resolution that it is increasingly important to capture relatively low Mach number features with the same compressible scheme. An example of such combined flows could include a super-critical aerofoil with a turbulent wake, shock-induced shear instabilities, or Rayleigh–Taylor instabilities.

In a recent paper [1], it was demonstrated that the leading order kinetic energy dissipation rate in a finite volume Godunov scheme increases as one over the Mach number. For the second-order of accuracy in space

☆ Contains material ©British Crown Copyright 2006/MOD.

* Corresponding author. Tel.: +44 1234 754796; fax: +44 1234 752149.
E-mail address: d.drikakis@cranfield.ac.uk (D. Drikakis).

0021-9991/$ - see front matter © 2008 Elsevier Inc. All rights reserved.
doi:10.1016/j.jcp.2008.01.036

'Monotone Upstream-centred Schemes for Conservation Laws' (MUSCL) method employing the van Leer limiter it was shown that the leading order kinetic energy dissipation rate ϵ^{VL} can be written as

$$\epsilon^{\mathrm{VL}} = \frac{\Delta x^2}{12} u u_x u_{xx} + \frac{\Delta x^3 a}{24}(3u_{xx}^2 + (2\mathcal{C}-3)u_x u_{xxx}), \tag{1}$$

where u and a are the velocity normal to the cell interface and speed of sound, respectively; $(.)_x$ indicates a derivative with respect to the direction normal to the cell interface; $\mathcal{C}$ is the Courant–Friedrich–Levy (CFL) number and Δx is the cell length (grid spacing). The dissipation rate is third-order in Δx as although the van Leer limiter is second-order accurate, the difference between the left and right extrapolated quantities at the cell interface is third-order. The key observations regarding this result is that the dissipation is proportional to the speed of sound and the magnitude of the velocity derivatives squared at leading order. Thus, any low Mach number features are heavily dampened by the numerical scheme.

Taking this into account, it has become important to understand the behaviour of compressible schemes not only in the traditional sense of resolving sharp discontinuities where the flow properties change slowly between one discontinuity and the next, but also in regions of continuous smooth change. This could be across a single vortex or in a fully turbulent flow field, where there are significant differences in flow properties in the space of several cells throughout the flow field.

The modification proposed in this paper is intended for use in flows with both compressible and low Mach number features, such that the time step size is not constrained by the low Mach number features. It includes a simple local modification to the reconstruction process which effectively removes the Mach number dependence of the leading order dissipation rate of kinetic energy, hence significantly improving the resolution of low Mach number portions of a compressible flow. It is applied in this paper to a Godunov-type method, however, in principle there is no reason why it cannot be extended to any compressible method which employs a reconstruction phase. The main feature of the modified numerical method proposed here is that it *locally* adapts the reconstruction method to allow good resolution of low Mach number features and shocks at the same time without modifying the formulation of the governing equations. The modification requires negligible additional computational expense.

The layout of this paper is as follows. Section 2 proposes a simple modification of the limiting method applied only to the velocity jumps across the cell interface. It is shown analytically that with the modification the leading order dissipation rate is constant as the Mach number tends to zero, instead of tending to infinity as with the original scheme. This method has been implemented in conjunction with a fifth-order in space and third-order in time MUSCL-based finite volume Godunov method, which is also detailed in Section 2. The original fifth-order method and the modified scheme are applied to several numerical testcases in Section 3. These testcases serve two purposes, firstly that the proposed modification does not compromise the shock capturing capability of the numerical method, and secondly that there is a significant improvement in resolution at low Mach number. Shock capturing capability is demonstrated via the Sod and Noh shock tube tests, and the simulation of advection via a weak acoustic wave in Section 3.1. Simulations of a two-dimensional Kelvin–Helmholtz instability in Section 3.2 demonstrate clearly that the modified reconstruction method extends the ability of the Godunov method to Mach numbers as low as 10^{-4} and recovers the expected M^2 scaling of pressure and density fluctuations. Two complex three-dimensional test cases are detailed in Section 3.3. The modified scheme is shown to significantly reduce dissipation at the high wave number modes in homogeneous decaying turbulence. It is then applied to a high resolution simulation of the Richtmyer–Meshkov instability, where the turbulent kinetic energy spectra are in excellent agreement with theoretical predictions, especially considering the lack of an explicit subgrid scale model. Finally, Section 4 presents the conclusions drawn from the present study and discusses the direction of future work.

2. Numerical method

2.1. Base numerical scheme

This paper is concerned with the simulation of the Euler equations, where viscosity is assumed negligible ($Re \to \infty$). The discretisation of the convective fluxes in each principal direction is obtained using the one-

dimensional counterpart of the three-dimensional compressible Euler equations,[1] e.g. for the flux $\mathbf{E}$ the following system is used,

$$\frac{\partial \mathbf{U}}{\partial t} + \frac{\partial \mathbf{E}}{\partial x} = 0, \tag{2}$$

where

$$\mathbf{U} = [\rho, \rho u, \rho v, \rho w, E]^{\mathrm{T}}, \tag{3}$$

$$\mathbf{E} = \left[\rho u, \rho u^2 + p, \rho uv, \rho uw, (E+p)u\right]^{\mathrm{T}}, \tag{4}$$

$$E = \rho e + 0.5\rho(u^2 + v^2 + w^2) \tag{5}$$

and ρ, e, u, v, w are the density, specific internal energy per unit volume and Cartesian velocity components, respectively. Throughout this paper it is assumed that the fluid satisfies the ideal gas equation of state

$$p = \rho e(\gamma - 1), \tag{6}$$

where γ is the ratio of specific heats. The Kelvin–Helmholtz and Richtmyer–Meshkov simulations also advect a passive scalar to track the two gas components, assumed to be miscible. The fluxes are obtained by solving the Riemann problem at the cell interface using left and right limited quantities. In this paper the HLLC approximate Riemann solver is employed as detailed in Toro [2]. Higher order accuracy is achieved using MUSCL extrapolation [3],

$$\mathbf{P}^{\mathrm{L}}_{i+1/2} = \mathbf{P}_i + \frac{1}{2}\phi^{\mathrm{lim}}(r^{\mathrm{lim,L}})(\mathbf{P}_i - \mathbf{P}_{i-1}), \tag{7}$$

$$\mathbf{P}^{\mathrm{R}}_{i+1/2} = \mathbf{P}_{i+1} - \frac{1}{2}\phi^{\mathrm{lim}}(r^{\mathrm{lim,R}})(\mathbf{P}_{i+2} - \mathbf{P}_{i+1}), \tag{8}$$

where $\mathbf{P}$ is the vector of cell averaged primitive variables and the cells are labelled by the integer i. Also,

$$r_i^{\mathrm{lim,L}} = \frac{\mathbf{P}_{i+1} - \mathbf{P}_i}{\mathbf{P}_i - \mathbf{P}_{i-1}}, \quad r_i^{\mathrm{lim,R}} = \frac{\mathbf{P}_i - \mathbf{P}_{i-1}}{\mathbf{P}_{i+1} - \mathbf{P}_i}. \tag{9}$$

The fifth-order limiter proposed by Kim and Kim [4] is employed

$$\Phi^*_{\mathrm{M5,L}} = \frac{-2/r_{i-1}^{\mathrm{lim,L}} + 11 + 24r_i^{\mathrm{lim,L}} - 3r_i^{\mathrm{lim,L}} r_{i+1}^{\mathrm{lim,L}}}{30}, \tag{10}$$

$$\Phi^*_{\mathrm{M5,R}} = \frac{-2/r_{i+2}^{\mathrm{lim,R}} + 11 + 24r_{i+1}^{\mathrm{lim,R}} - 3r_{i+1}^{\mathrm{lim,R}} r_i^{\mathrm{lim,R}}}{30}, \tag{11}$$

where monotonicity is maintained by limiting the above extrapolations using

$$\phi^{\mathrm{lim}}_{\mathrm{M5,L}} = \max(0, \min(2, 2r_i^{\mathrm{lim,L}}, \Phi^*_{\mathrm{M5,L}})), \tag{12}$$

$$\phi^{\mathrm{lim}}_{\mathrm{M5,R}} = \max(0, \min(2, 2r_i^{\mathrm{lim,R}}, \Phi^*_{\mathrm{M5,R}})). \tag{13}$$

This completes the description of the standard fifth-order method which will be denoted as 'M5' throughout this paper. The fifth-order method gives significantly better resolution than typical second-order schemes, for example, in the Sod shock tube case the extent of diffusion of the contact surface is typically reduced by one third compared to MUSCL with the second-order van Leer limiter.

As shown by Guillard et al. [5] the scaling of the pressure differences is incorrect at low Mach number for the standard Godunov scheme. This can be shown by examining the solution to the Riemann problem for the interface pressure, where

$$p = p + \frac{M}{2}\sqrt{\gamma p \rho}\Delta u \tag{14}$$

at the cell interface once the Riemann problem is solved. The theoretical analysis in Thornber et al. [1] demonstrated that this is caused by the specification of an artificially large velocity jump at the cell interface when using piecewise constant variable extrapolation.

[1] The discretised flux derivatives are summed and then advanced in time obtained using a Runge–Kutta scheme.

The solution to this problem can be approached in two different ways. One method would be to modify the Riemann solver itself in an attempt to compensate for the strength of the acoustic waves. This approach would lead to a preconditioned method such as that proposed by Guillard *et al* [5], or a modification of the wave strengths in the Roe scheme as suggested by Thornber and Drikakis [6]. However, a second approach is to consider that the Riemann solver is acting upon artificially large jumps in the primitive variables. These jump sizes have been determined through purely mathematical reasoning (i.e. via extrapolation at a specified order of accuracy of cell centred quantities) without regard for the physical nature of the flow being simulated. In this paper it is proposed to modify the extrapolated or 'limited' quantities in order to take into account the flow physics at low Mach numbers.

2.2. Modified reconstruction method

As has been demonstrated analytically in [1], the kinetic energy dissipation rate can be gained by analysis of the generation of entropy over a single time step, using the Taylor series expansion of the extrapolated variables. This is based on the observation that in the absence of strong thermal conduction, the generation of entropy change by temperature is equal to the dissipation of kinetic energy.

The Taylor series expansion of MUSCL reconstruction using the M5 interpolation method on the vector of cell averaged primitive variables $\mathbf{P}$ gives

$$\widetilde{\mathbf{P}}(x) = \mathbf{P}^i + \frac{\Delta x}{2}\mathbf{P}^i_x + \frac{\Delta x^2}{12}\mathbf{P}^i_{xx} - \frac{\Delta x^4}{720}\mathbf{P}^i_{xxxx} + \frac{\Delta x^5}{60}\mathbf{P}^i_{xxxx} + \ldots, \tag{15}$$

where $\mathbf{P}^i$ indicates functions evaluated at the cell centre. The exact expansion from the cell averaged quantity to the continuous function gives

$$\mathbf{P}(x) = \mathbf{P}^i + \frac{\Delta x}{2}\mathbf{P}^i_x + \frac{\Delta x^2}{12}\mathbf{P}^i_{xx} + \frac{\Delta x^2}{12}\mathbf{P}^i_{xx} - \frac{\Delta x^4}{720}\mathbf{P}^i_{xxxx} + \mathcal{O}(\Delta x^6), \tag{16}$$

confirming that the extrapolation method is fifth-order accurate. From this point on the superscripts $(.)^i$ will be omitted for clarity. It was shown in [1] that the leading order dissipation rate arises due to the velocity jump normal to the cell interface. Thus, for simplicity, a flow field consisting of constant density, pressure and shear velocities but continuously varying normal velocity component u is considered. The following derivation is complex even for first-order in time and space methods, hence following verification of the methodology (detailed in [1]), a Mathematica script was used for the analysis. This Mathematica script is included in Appendix, so that interested readers can repeat the analysis.

The fluxes at the $i + 1/2$ and $i - 1/2$ interfaces are computed from the Taylor series expansion of the M5 extrapolation. These are then evolved at first-order in time and the change of entropy over the time step computed. Next, this process was repeated using the exact solution at the cell interfaces (i.e. the same process, but with the exact Taylor series expansion). The leading order change in entropy in the discrete solution with van Leer limiting is then subtracted from the exact solution, giving the kinetic energy dissipation rate due to the errors in the spatial discretisation. Remarkably, this consists of only a single term

$$\epsilon^{\mathrm{M5}} = \frac{\Delta x^5}{60} a u_x u_{xxxxx} + \mathrm{H.O.T.} \tag{17}$$

This term is proportional to Δx^5 as expected from the leading order of the difference between the left and right quantities in the expansion of the limiting function. Additionally, the dissipation rate increases with speed of sound a, as was previously demonstrated for the van Leer limiter [1].

A simple solution to the problem of the excessive numerical dissipation is sought by modifying the velocity jump at the cell interface by a function z, where the reconstructed velocities $\mathbf{u}$ are now defined by

$$\begin{aligned}
\mathbf{u}_{\mathrm{L,M5+LM}} &= \frac{\mathbf{u}_{\mathrm{L}} + \mathbf{u}_{\mathrm{R}}}{2} + z\frac{\mathbf{u}_{\mathrm{L}} - \mathbf{u}_{\mathrm{R}}}{2}, \\
\mathbf{u}_{\mathrm{R,M5+LM}} &= \frac{\mathbf{u}_{\mathrm{L}} + \mathbf{u}_{\mathrm{R}}}{2} + z\frac{\mathbf{u}_{\mathrm{R}} - \mathbf{u}_{\mathrm{L}}}{2}.
\end{aligned} \tag{18}$$

Repeating the above analysis for the new modified velocity extrapolation given by Eq. (18) yields,

$$\epsilon^{\mathrm{M5+LM}} = \frac{\Delta x^5}{60} z a u_x u_{xxxxx} + \mathrm{H.O.T.}, \tag{19}$$

where H.O.T. are higher order in terms of spatial derivative, but lower order in terms of speed of sound. It can be seen that by choosing $z = \min(M_{\mathrm{local}}, 1))$, $M_{\mathrm{local}} = \max(M_{\mathrm{L}}, M_{\mathrm{R}})$ the leading order dissipation rate becomes

$$\epsilon^{\mathrm{M5+LM}} = \frac{\Delta x^5}{60} \min(|u|, a) u_x u_{xxxxx} + \mathrm{H.O.T.} \tag{20}$$

This ensures that the dissipation does not exceed that of the original scheme and reverts to the standard upwind form in supersonic flows. Several other forms of the function z have been investigated, including quadratic functions of M, varying the cut-off Mach number and the linear rate of decrease of z with respect to Mach number. However, as well as being the simplest, the form proposed here also gives the best results in terms of uniformity of dissipation at low Mach number in numerical test cases.

The new treatment of the velocity jumps can be considered more 'realistic', in that the standard Godunov method sets up artificially large jumps which would not be present in a low Mach number flow field. It can also been seen as a progressive central differencing of the velocity components as Mach number tends to zero. The left and right densities or pressures are not modified, as this will cause excessive diffusion in stationary contact surfaces, which is not desirable. Importantly, as the sign of the fifth derivative is the same as the sign of the first derivative, the leading order term is still absolutely dissipative locally. A key observation is that the reconstruction is modified based on the local properties of the flow field, hence the same governing equations are solved throughout the domain.

By assuming that the flow field in subsonic and consists of a single sinusoidal perturbation, where $u(x) = \tilde{u}\sin(kx)$ and $k = 1/n\Delta x$, the dissipation rate can be written as

$$\epsilon^{\mathrm{M5+LM}} \approx \frac{1}{60n^6} \frac{|\tilde{u}|^3}{\Delta x}, \tag{21}$$

which shows a similar functional form to Kolmogorov's four-fifths law (which gives $\epsilon \propto |u|^3/l$), whereas the standard method gives a dissipation rate of the form $\epsilon \propto u^2 a/\Delta x$. This paper includes some fully turbulent test cases to investigate if this functional change in the dissipation rate improves performance in the framework of Implicit Large Eddy Simulation. From the above it is clear that the dissipation rate decreases steeply as n increases (as the wavelength of the mode under consideration increases) as is expected of a higher order method.

The leading order dissipation rate gives increasing entropy as long as the standard CFL criteria is held, thus the numerical method does not suffer the severe instability of preconditioned methods when used in conjunction with explicit time stepping [7]. Additionally, substituting the modified velocity jump according to Eq. (18) into Eq. (14) recovers the expected M^2 scaling of the pressure and density variations. This numerical method is denoted 'M5+LM' throughout this paper.

It should be noted that not all interpolation methods can be modified in this way. A similar modification applied to the van Leer limiter gives a leading order truncation error

$$\epsilon^{\mathrm{VL+LM}} = \frac{\Delta x^2}{12} u u_x u_{xx} + \frac{\Delta x^3}{12} \mathcal{C} a u_x u_{xxx}, \tag{22}$$

demonstrating that one of the leading order terms still increases with speed of sound.

Finally, third-order accurate Runge–Kutta time stepping method is employed [8]

$$U_i^1 = U_i^n + \frac{1}{2}\frac{\Delta t}{\Delta x} f(U_i^n), \tag{23}$$

$$U_i^2 = U_i^n + \frac{1}{2}\frac{\Delta t}{\Delta x} [f(U_i^1)], \tag{24}$$

$$U_i^{n+1} = \frac{1}{3}\left(2U_i^2 + U_i^n + \frac{\Delta t}{\Delta x}[f(U_i^2) + f(U_i^1)]\right), \tag{25}$$

where $f(U_i^n)$ indicates the net flux into the cell evaluated using the array of conserved variables at time n in cell position i (see also [9]). This has an extended stability region to a theoretical limit of CFL = 2.

3. Test cases

Several test cases are now presented to examine numerically the properties of the modified reconstruction method, and to verify the results of the theoretical analysis within the previous section. Firstly, one-dimensional problems are employed to verify that the modification does not compromise the ability of the scheme to capture shock waves, and to resolve acoustic waves. Next, a two-dimensional, single mode Kelvin–Helmholtz instability is simulated to demonstrate clearly the significantly improved resolution of the modified method at low Mach numbers compared to the standard fifth-order method. Finally, two complex three-dimensional flows are simulated to demonstrate the applicability of the proposed method to unsteady, compressible turbulent flows which have both compressible and incompressible features.

3.1. One-dimensional test cases

3.1.1. Modified Sod shock tube

To demonstrate that the proposed modification does not affect the ability of the scheme to capture shock waves and contact surfaces the original and modified method have been applied to the Sod shock tube test case modified to include stationary flow within the rarefaction fan. This modification is used to test the scheme for unphysical rarefaction shocks when the leading order dissipation is decreased significantly within the fan. The initial conditions are

$$(\rho, u, p)_{\mathrm{L}} = (1, -0.5, 1), \quad (\rho, u, p)_{\mathrm{R}} = (0.125, 0, 0.1), \quad \gamma = 1.4 \tag{26}$$

where the initial discontinuity is placed at $x = 0.5$. The domain is of length 1 and was discretised using 100 cells. The CFL number was chosen as 1.4, and the results were taken at $t = 0.17$. Fig. 1 shows the pressure, density and velocity profiles using both the modified and original limiting methods. The pressure and density profiles are almost indistinguishable from the original fifth-order scheme. There is only a slight change in position of the first point in the shock wave and the modified scheme gives sharper profiles at the head and tail of the rarefaction.

3.1.2. Density layer

The second test case is taken from Klein [10] and is used to validate that the scheme can advect large density variations at $M = 0.02$ at very low dissipation, whilst resolving a low wavelength acoustic wave which passes through the density layer. The initial conditions are defined by

$$\rho(x, 0) = 1 + \Phi \sin(40\pi x/L) + M(1 + \cos(\pi x/L)), \tag{27}$$

$$p(x, 0) = 1 + \gamma M(1 + \cos(\pi x/L)), \tag{28}$$

$$u(x, 0) = \sqrt{\gamma} M(1 + \cos(\pi x/L)) \tag{29}$$

and the domain size is $-L \leqslant x \leqslant L = 1/M$ where $M = 1/51$. Finally, the domain is discretised with 1020 points, CFL = 1.4, and $\gamma = 1.4$. Fig. 2 shows the pressure, velocity and density distributions at time $t = 5.071$ for both the original fifth-order scheme and the modified scheme, corresponding to about two and a half passages of the long wave acoustic perturbation. Again, both modified and unmodified schemes perform extremely well, the total density variation has been reduced by only 7% compared to the initial amplitude. The total density variation initial and modified scheme vary by only $10^{-3}\%$. This is far better than the Superbee results reported in [10] and as good as the low dissipation implicit scheme presented there. This was the only test case examined here where the modified scheme was less robust than the original scheme, which would run up to CFL = 1.6.

3.1.3. Noh

The third test case is taken from Noh [11] and consists of two infinite strength shocks moving out from the centre. This is employed to test the performance of the scheme for very strong shocks. The initial conditions are

$$(\rho, u, p)_{\mathrm{L}} = (1, 1, 10^{-6}), \quad (\rho, u, p)_{\mathrm{R}} = (1, -1, 10^{-6}), \quad \gamma = 5./3., \tag{30}$$

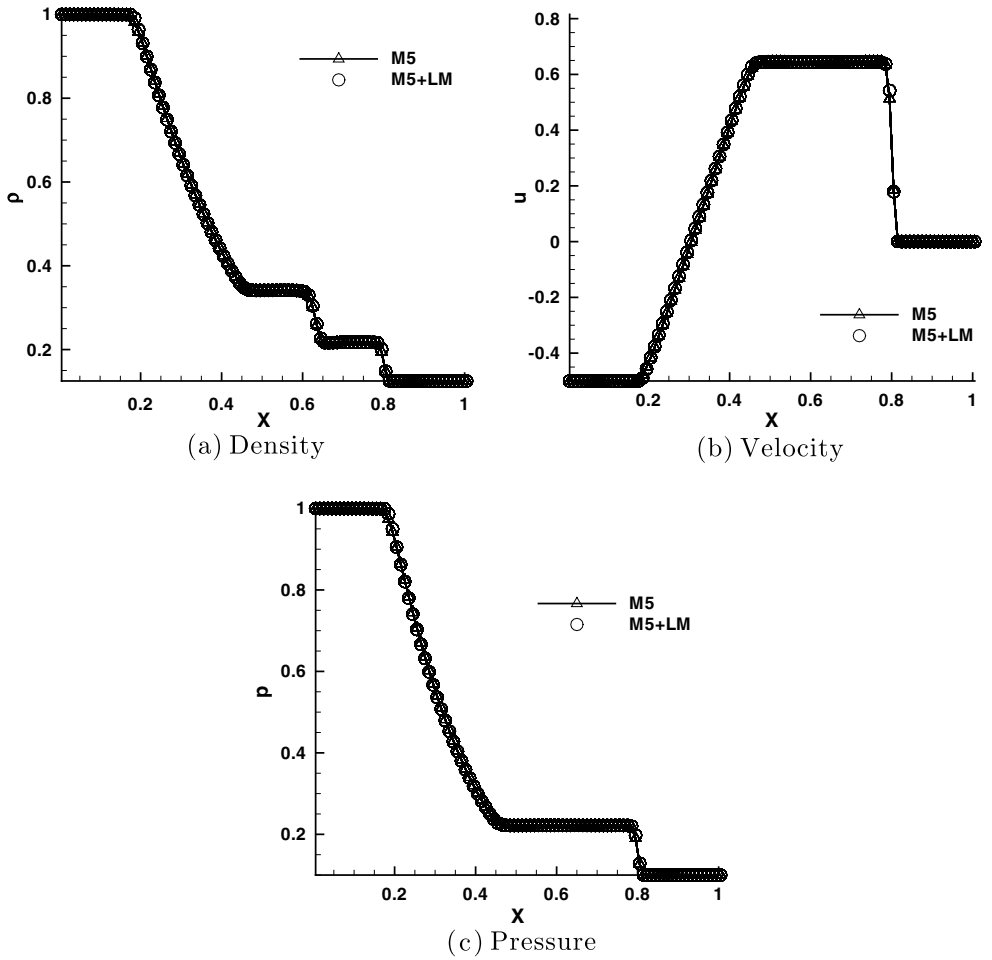

Fig. 1. Results from the modified Sod shock tube test case.

where the initial discontinuity is placed at $x = 0.5$. The domain is of length 1 and was discretised using 100 cells. The CFL number was chosen as 1.5, and the results were taken at $t = 1$. Fig. 3 shows the density profiles using both the modified and original limiting methods. Both original and modified schemes demonstrate excellent shock capturing, however both schemes break symmetry (as do many high order schemes in this test case (see Liska and Wendroff [12]), and are oscillatory behind the strong shock. Performance in this test case can be improved by employing TVD time stepping method. This is demonstrated in Fig. 4, which shows the results gained with the same reconstruction method but employing the third-order TVD Runge–Kutta time stepping of Gottlieb and Shu [13] at CFL 0.5. The spread of the oscillations away from the centre is significantly reduced for both reconstruction methods, with the modified scheme giving the best results in the uniform region behind the shock.

3.2. Two-dimensional test cases

3.2.1. Single mode Kelvin–Helmholtz

The effective resolution of a numerical scheme can be determined by examining the ability to resolve the a single mode instability. In this case, an initially small perturbation velocity of one tenth the free stream Mach number triggers the development of a Kelvin–Helmholtz vortex. It is initialised following [14]

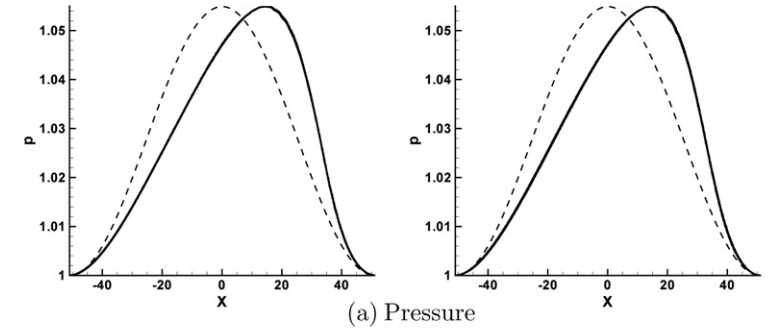

(a) Pressure

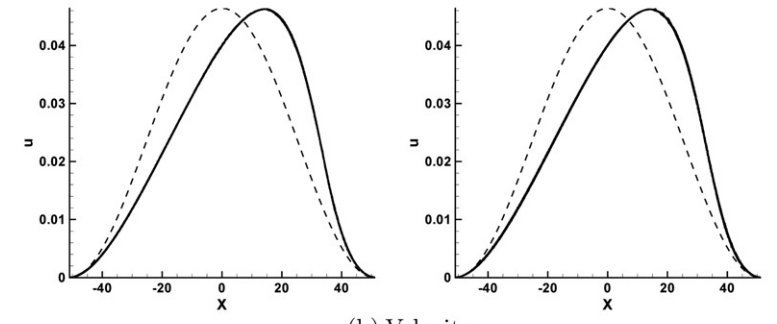

(b) Velocity

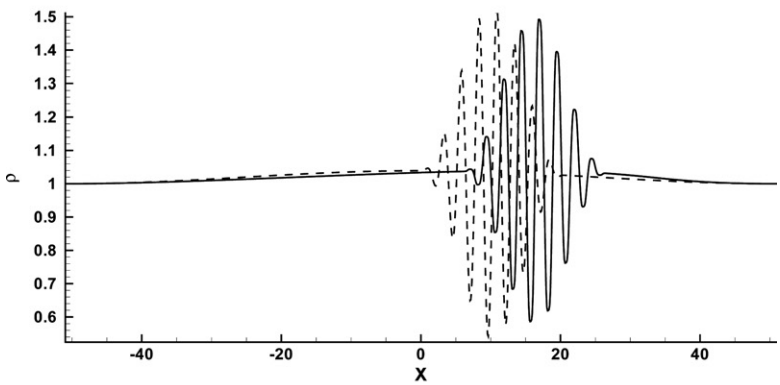

(c) Density M5

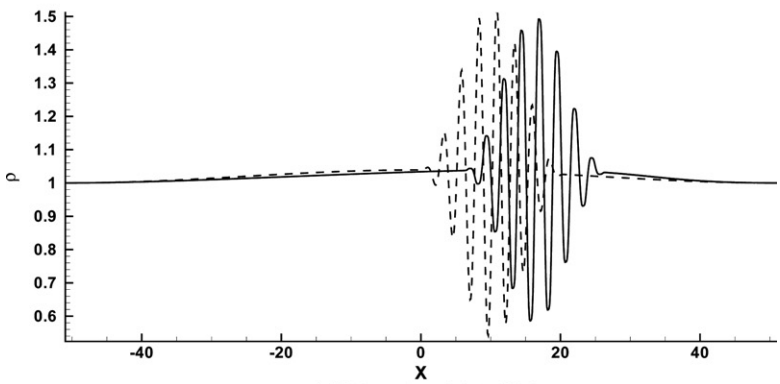

(d) Density M5+LM

Fig. 2. Results from the density layer test case, left column M5, right column modified scheme M5+LM. The initial conditions are shown as dashed lines.

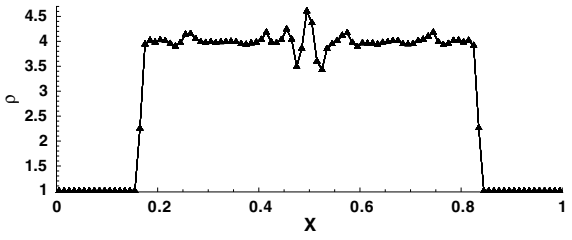
ρ
X

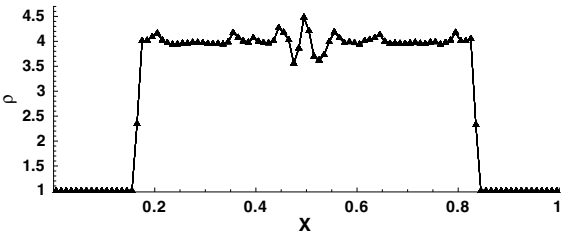
ρ
X

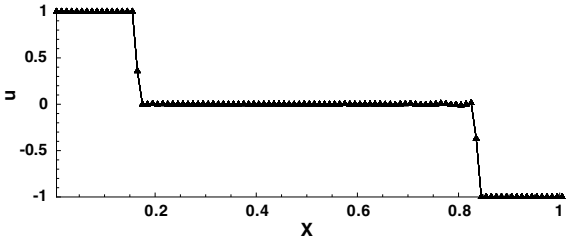
u
X

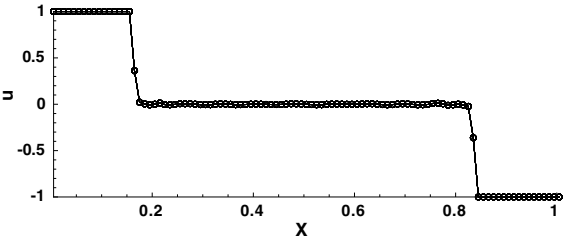
u
X

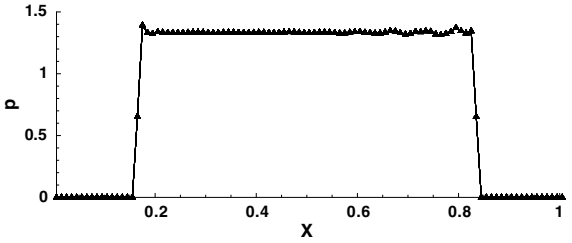
p
X

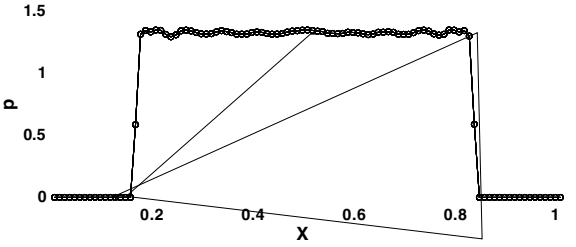
p
X

$$u = \frac{\partial A_z}{\partial y}, \quad v = -\frac{\partial A_z}{\partial x}, \quad A_z = \frac{V_0}{k}\cos(ky)\exp^{-k|x|}, \quad V_0 = 0.1\Delta V, \tag{31}$$

where ΔV is the difference in mean flow velocity V across the mixing layer. In this example $\Delta V = 1$, hence $v = -\Delta V/2$ for $-0.5 < x < 0$ and $v = \Delta V/2$ for $0 < x < 0.5$. The Mach number, defined by $\Delta V/a$, is adjusted by changing the pressure. Density is fixed at $\rho = 1$, and $\gamma = 5/3$. The size of the domain is 1×1 and is discretised with 16 cells in each direction. The coarse resolution is deliberately chosen to highlight the scheme's ability to capture what would be a high wave number perturbation on a larger grid. It also allows easy demonstration of the low Mach number behaviour of the dissipation of kinetic energy.

Fig. 5 shows the development of the single mode vortex using the original fifth-order method at $M = 0.2$. The characteristic rolled up vortex is clearly visible, highlighted by the transport of a passive scalar into the spirals. It should be noted that this is already a reasonable result – using a second-order limiter such as van Leer at this grid resolution would give no visible roll-up.

If the Mach number is reduced by increasing the background pressure, then excessive dissipation prevents growth of the initial instability. Fig. 6 shows the development of the mixing layer at $M = 0.02$ and 0.002. At flow Mach numbers of less than 0.2 the perturbation is dissipated, preventing the growth of the instability.

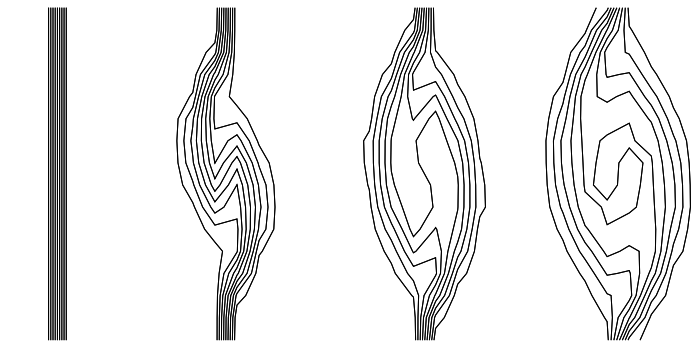

Fig. 5. Contour lines at mass fraction 0.1 through to 0.9 with increments of 0.1 showing the development of the KH instability at Mach = 0.2 using scheme M5.

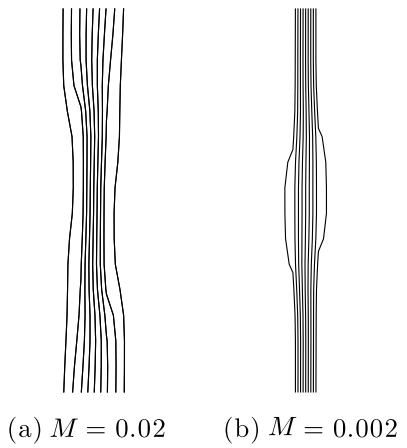

Fig. 6. Contour lines at mass fraction 0.1 through to 0.9 with increments of 0.1 at $t = 3$ for Mach numbers 0.02 and 0.002 using scheme M5.

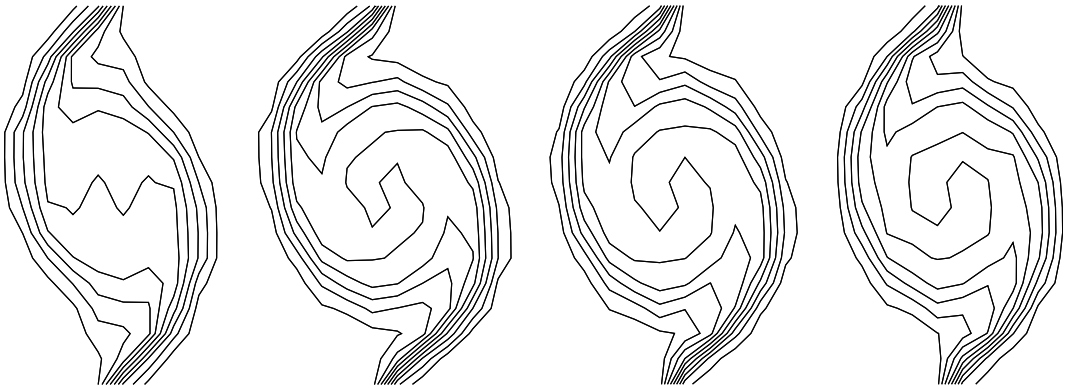

(a) $M = 0.2$ (b) $M = 0.02$ (c) $M = 0.002$ (d) $M = 0.0002$

Fig. 7. Contour lines at mass fraction 0.1 through to 0.9 with increments of 0.1 using M5+LM at $t = 3$.

Applying the low Mach number correction to the velocity jumps improves the resolution of the perturbation, as shown in Fig. 7. At $M = 0.2$ the vortex roll-up is greater, however, the 0.5 contour line has merged in the central cells thus creating the 'kink' in vortex centre. As Mach $\to 0$ the spiral structure of the vortex is perfectly intact and appears to be reaching a relatively Mach number independent structure. At the lowest Mach number there is a very slight asymmetry in the results, which is due to the use of a small number to prevent a division by zero in the limiting stage of the calculation.

As pointed out in Guillard et al. [15,5] it is important that the pressure and density fluctuations follow the correct scaling. They demonstrate clearly that the standard finite volume scheme contains pressure fluctuations of order M, contrary to the incompressible limit which should only support perturbations of order M^2. The relative pressure and density difference are defined as

$$\Delta p = \frac{p_{\max} - p_{\min}}{p}, \quad \Delta\rho = \rho_{\max} - \rho_{\min}, \tag{32}$$

and are plotted in Fig. 8 for $M = 0.2$ to $M = 0.0002$ at $t = 3$ for scheme M5+LM. Below Mach numbers of 0.2 the maximum pressure variation follows a M^2 scaling as required from incompressible theory, as does the scaling of density variation.

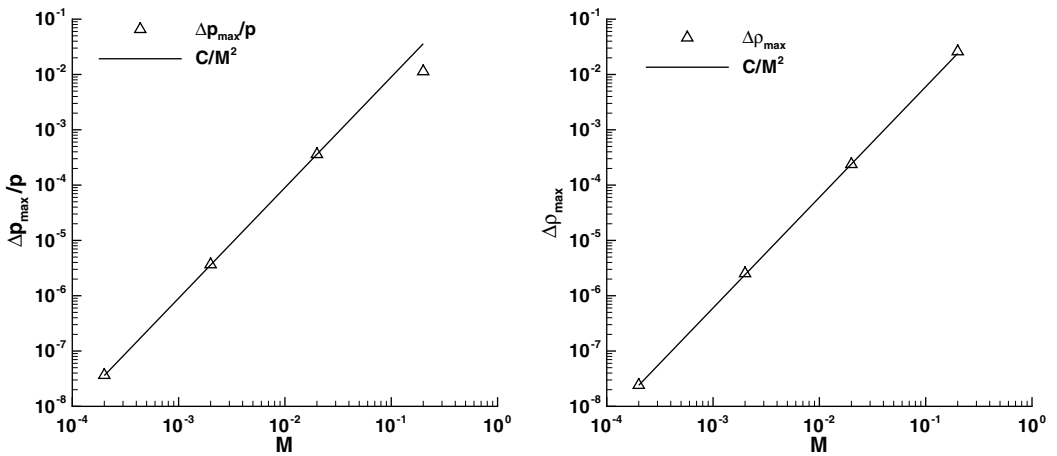

(a) Pressure (b) Density

Fig. 8. Scaling of the maximum pressure and density variations with Mach number at $t = 3$ for scheme M5+LM.

3.3. Three-dimensional test cases

3.3.1. Homogeneous decaying turbulence

In this section the schemes are tested for the ability to resolve a turbulent flow, where all flow properties vary continuously throughout the flow field. The canonical numerical test case for which theoretical results are available for comparison is that of homogeneous decaying turbulence in a periodic cube. From the results in Section 3.2.1 it is expected that the modified scheme will be significantly less dissipative. This would be a great advantage as it is well known that Godunov schemes dissipate heavily at high wave numbers [16,17].

The flow field was initialised using a method derived by Youngs and utilised in previous simulations of decaying turbulence [18,19,17]. The flow field has an initial kinetic energy spectrum given by [20]

$$E(k) = u'^2 \frac{k^4}{k_\mathrm{p}^4} \sqrt{\frac{8}{k_\mathrm{p}^2 \pi}} \exp(-2(k/k_\mathrm{p})^2), \tag{33}$$

where k is the wave number, and the peak in the energy spectrum is defined by changing the peak k_p in the exponential. The peak of the energy spectrum was chosen at $k_\mathrm{p} = 4$. To ensure the generation of an almost non-divergent (i.e. incompressible) velocity field, the velocity is formed from components of a vector potential A, which satisfies the following relationship:

$$u = \nabla \times A. \tag{34}$$

As the divergence of a curl is identically equal to zero this gives a non-divergent velocity field. The vector potential is initialised with a Gaussian distribution of amplitudes and random phases, which is rescaled linearly to give a velocity field satisfying

$$KE = \frac{3}{2} u^2 = 0.5, \tag{35}$$

$$M = \frac{u}{c} = 0.1, \tag{36}$$

where u is the mean turbulent velocity. The chosen Mach number is low for a Godunov method, and thus it highlights more clearly the advantages of the modified MUSCL reconstruction proposed. The simulations were run at 32^3, 64^3 and 128^3 using both M5 and M5+LM, and the viscous terms were neglected ($Re = \infty$). Fig. 9 plots the mean kinetic energy per cell versus time for each grid resolution up to $t = 5$ which corresponds to about eight eddy turnover times. At lower grid resolutions the M5+LM scheme resolves more kinetic energy, and begins decay at a later time, which is a typical feature of increased resolution of the scheme. Fig. 9d compares the kinetic energy decay rate of the 32^3 modified scheme with the performance of the 64^3 scheme showing that the modified scheme behaves very close to the unmodified scheme at double the resolution.

Three-dimensional kinetic energy spectra have been calculated following [21]

$$E(k) = 2\pi k^2 \phi_{ii}(k), \tag{37}$$

where $k = \sqrt{k_x^2 + k_y^2 + k_z^2}$ and the spectrum tensor ϕ is

$$\phi_{ij}(\mathbf{k}) = \frac{1}{(2\pi)^3} \int_{-\infty}^{\infty} Q_{ij}(\mathbf{r}) \mathrm{e}^{-\mathrm{i}\mathbf{k}\mathbf{r}} \mathrm{d}\mathbf{r}, \tag{38}$$

where Q_{ij} is the second-order velocity correlation tensor. The instantaneous three-dimensional energy spectra are shown in Fig. 10 for several time instants using both methods at each resolution. The original method shows the dissipative nature of the unaltered Godunov method for high wave number modes. There is a significant improvement in the turbulent spectra at all grid resolutions indicating much higher energy in the high wave numbers when modifying the velocity increments at low Mach number. The original numerical dissipation was clearly too high (due to the speed of sound dependence) and thus generated a much larger dissipation range than desirable when simulating turbulent flow. There is a good match to a $k^{-5/3}$ spectrum when using the modified scheme despite there being no subgrid model employed – indicating that the modified scheme is potentially a good candidate for Implicit Large Eddy Simulation (ILES).

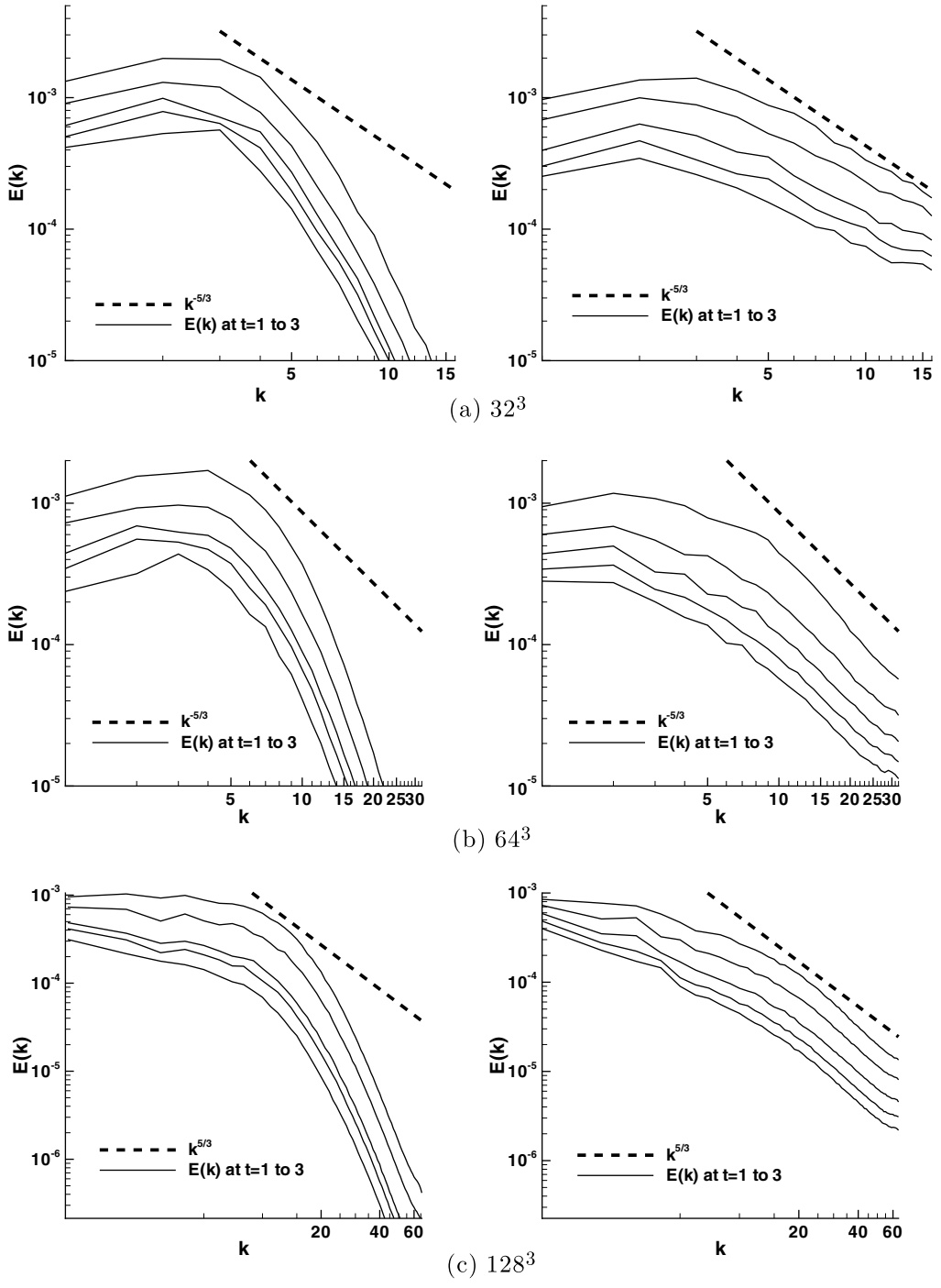

Fig. 10. Instantaneous three-dimensional energy spectra taken at $t = 1$ to 3 in increments of 0.5, where the highest solid line is the earliest time. Results for M5 are in the left column, M5+LM in the right column.

$$v_n = \frac{T(k,t^n) - (E(k,t^{n+1}) - E(k,t^{n-1}))/2\Delta t}{2k^2 E(k,t^n)}, \tag{41}$$

where modes are included in the computation only if the magnitude of the wave vector is smaller than a cut-off wave number k_c. It is normalised using the energy at the cutoff wave number $E(k_c)$ and k_c

$$v_n^+(k|k_c) = \frac{v_n}{\sqrt{E(k_c)/k_c}}. \tag{42}$$

This is compared to the theoretical result, gained via the test field model and eddy damped quasi-normal Markovian approximation, fitted by the expression of Chollet [23]

$$v_n^+(k|k_c) = C_K^{-3/2}\left(0.441 + 15.2e^{-3.03k_c/k}\right). \tag{43}$$

Fig. 11 shows the effective spectral eddy viscosity for the modified and unmodified scheme compared to the 'ideal' form. Both methods follow the same qualitative trends, in that they have a plateau at moderate wave numbers, gradually increasing to a 'cusp' at the defined cut-off wave number (in this case half the maximum wave number on the grid). The modified method provides a much better match to the theoretical result, with a spectral eddy viscosity between 2 and 7 times less at a given wave number.

3.3.2. Richtmyer–Meshkov mixing

Finally the numerical scheme is applied to a three-dimensional mixing problem where the sharp and accurate treatment of shock waves and contact surfaces is of paramount importance. Richtmyer–Meshkov mixing is generated when a perturbed interface between two gases is impulsively accelerated, typically by a shock wave [24,25]. These instabilities first grow linearly and then transition to turbulence and are of importance in the study of supernovae explosions, wakes of jet engines, combustion chambers and inertial confinement fusion. This type of interaction is typically at very high Reynolds numbers thus the viscous terms are neglected.

The test case uses the initial conditions derived by Youngs [26] to examine the influence of initial conditions on the growth of the resultant mixing layer. The flow field consists a heavy and light gas separated by a perturbed interface, where the perturbation satisfies a given power spectrum and mean amplitude. The incident shock wave is of $M = 1.84$, equivalent to a four-fold pressure increase across the shock wave. The domain chosen is of size $[0, 0, 0] \times [2.4\pi, 2\pi, 2\pi]$, where additional length is given in the x-direction to allow for growth of the mixing layer. The initial conditions are

$$x < 2.3 \quad (\rho, u, p) = (6.375, -61.4875, 4 \times 10^5), \tag{44}$$

$$2.3 < x < 3.35 + \xi \quad (\rho, u, p) = (3.0, -291.575, 10^5), \tag{45}$$

$$3.35 + \xi < x \quad (\rho, u, p) = (1.0, -291.575, 10^5), \tag{46}$$

where an initial velocity is given to the material interface such that the centre of the interface is stationary after passage of the shock wave. The ratio of specific heats, γ, is set to 5/3. The initial interface perturbation ξ is

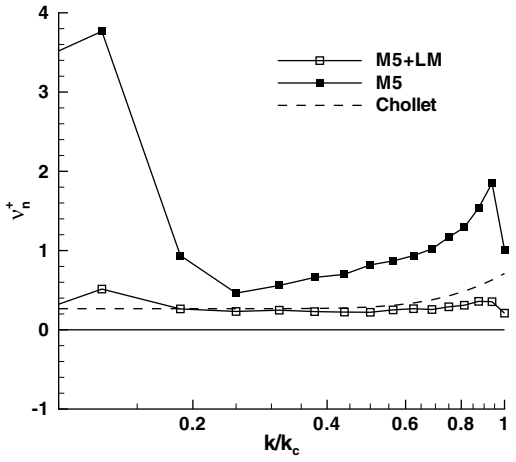

Fig. 11. Effective spectral eddy viscosity for the 64^3 simulation, where $k_c = 16$.

given as the sum of modes of random phase conforming to an initial power spectrum $P \propto c/k^2$. The modes excited are restricted between $\lambda_{\min} = 16\Delta x$ and $\lambda_{\max} = 2\pi/3$ and the standard deviation of the perturbation amplitude is $0.1\lambda_{\min}$. Fig. 12 shows the isosurface of mass fraction $Y_1 = 0.5$ at $t = 0$, illustrating the nature of the perturbation. The grid size employed is $360 \times 300 \times 300$ and simulations were run with both the original M5 limiter and modified M5+LM scheme at CFL = 0.75.

Once the shock wave has passed, the maximum Mach number within the mixing layer is approximately 0.25 and decreases with time, thus the standard boundary conditions utilised in a compressible code cannot be applied in the x direction. To prevent excessive reflection of the incident and reflected shock wave, an extended one-dimensional domain is employed as inlet and outlet conditions in the x direction. This does not completely eliminate the reflected wave as this is impossible where the mesh size changes (see [27]), but reduces the magnitude of the reflected wave to 0.03% of the initial velocity, which is then transmitted without reflection through the inlet boundary condition. In the y and z direction periodic boundaries are applied. Note that in the following discussion all length scales are non-dimensionalised by $\lambda_{\min}$, time scales by $\lambda_{\min}$ and $\Delta u = 291.575$ (the initial velocity impulse applied to the interface by the shock wave).

Fig. 13 shows three time instances in the development of the mixing layer for each scheme. The large scale structures are in similar locations in both of the schemes, however, it is clear that there is significantly improved resolution of fine scale features, as expected from the previous test cases. Fig. 14 shows a plane slice of the domain showing contours of mass fraction at $t = 240$ for both numerical schemes, further highlighting the increased resolution of the modified scheme.

Next the growth of the mixing layer is examined. It is expected that the mixing layer integral width, defined as

$$W = \int_x \bar{f}_1 \bar{f}_2 \, \mathrm{d}x, \tag{47}$$

where f_1 and f_2 are the volume fractions of the two gases, should grow as t^θ. Theoretical analysis suggests that at late times $\theta \approx 1/3 - 2/3$ [28–30]. Fig. 15 shows the non-dimensional mixing layer width. The lines of best fit show $\theta \approx 0.35$ for the original scheme and $\theta \approx 0.38$ for the modified scheme, in reasonable agreement. The increased resolution of fine scale structure does not significantly affect the integral mixing layer width, which

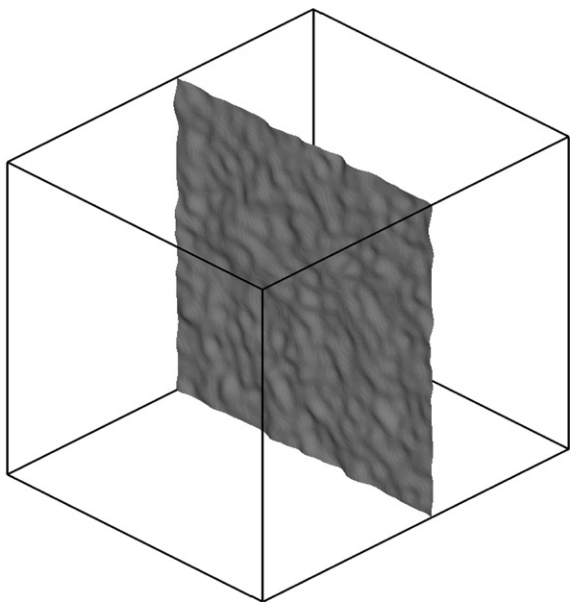

Fig. 12. Iso-surface of mass fraction $Y_1 = 0.5$ illustrating the initial condition for the Richtmyer–Meshkov test case.

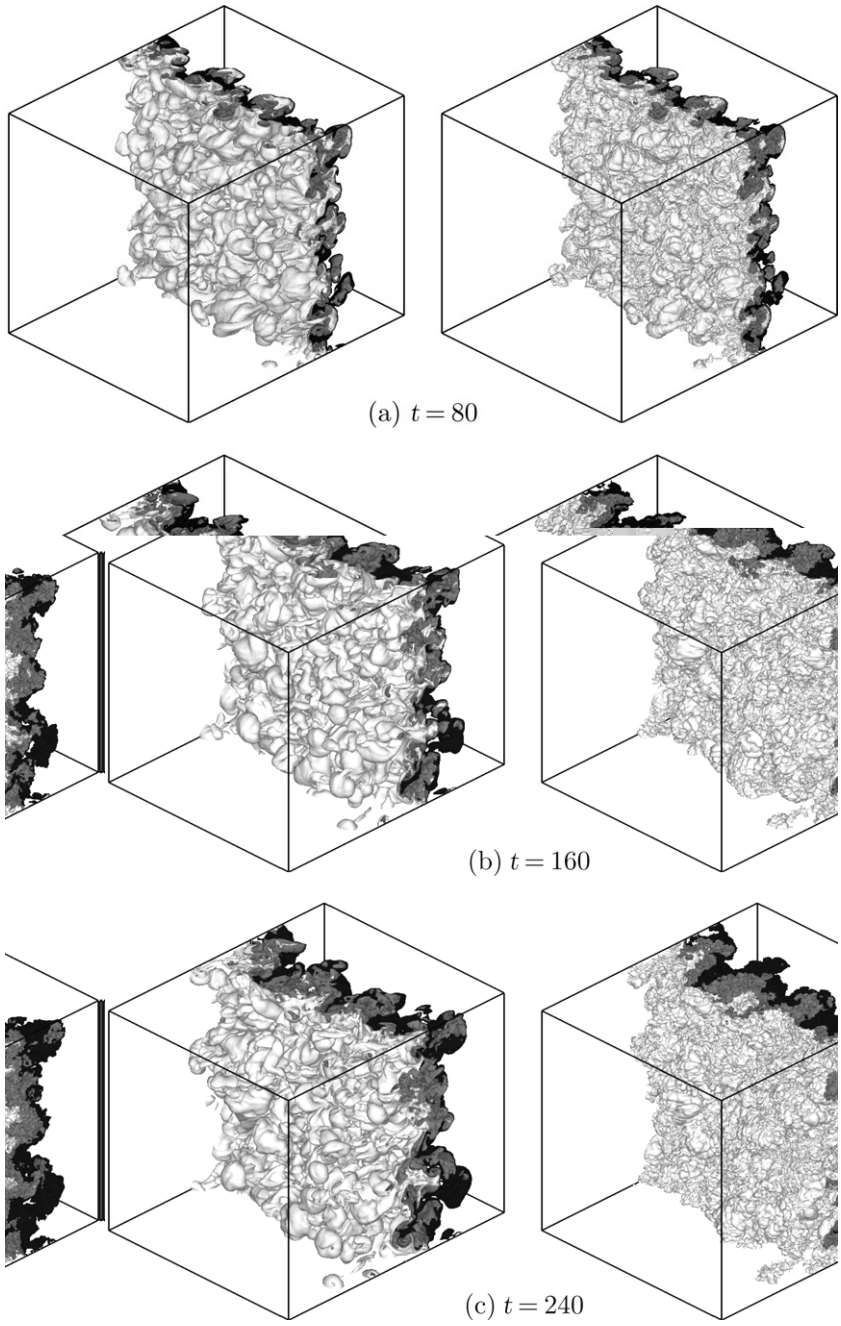

Fig. 13. Iso-surface of mass fraction $Y_1 = 0.05, 0.5$ and 0.95 showing the time development of the turbulent mixing layer. Results for M5 are in the left column, M5+LM in the right column.

is to be expected as simulations with single mode perturbations demonstrate that the mixing layer width can usually be captured on a very coarse grid [31].

Finally, the two-dimensional turbulent kinetic energy spectra has been calculated in the $y - z$ plane (parallel to the initial interface) and averaged over 10 slices in the x direction (direction of shock propagation). Each spectra is computed for a slice 256 by 256 and the 10 slices are symmetric across the centre of the mixing layer. Fig. 16 compares the spectra obtained using the two numerical methods at several time instances during the

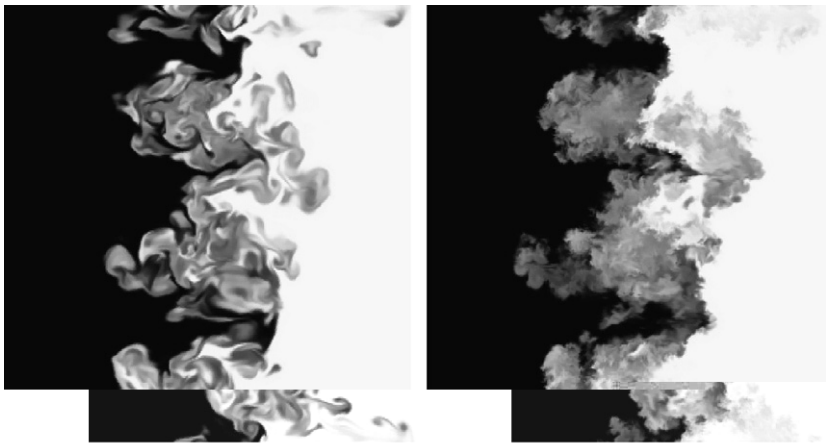

Fig. 14. Contour flood of mass fraction at $t = 240$ illustrating the fine scale structures present.

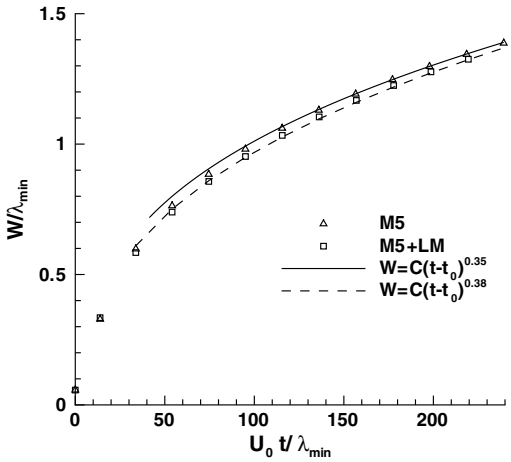

Fig. 15. Variation of the integral mixing width W with time for the two numerical schemes.

decay of turbulent kinetic energy. A $k^{-3/2}$ line has been plotted on the charts which is the theoretical form of the turbulent kinetic energy spectra determined by extending the Kolmogorov–Kraichnan phenomenology to take into account the 'driven' nature of the turbulent mixing zone [29].

There is an excellent match between the theoretical result and the M5+LM scheme between $8 < k < 100$, indicating that excess dissipation at low Mach number effectively removed small perturbations from the original fifth-order scheme thus preventing development of a fully turbulent flow regime. This is an excellent result, especially considering the lack of an explicit subgrid model, and a huge improvement on the original scheme. To the author's knowledge, such a large inertial range has not been seen in simulations less than 1024^3 [32] with other high resolution schemes. Further analysis as regards the form of the effective subgrid model in this case is a subject of ongoing work. It could be suggested that there is a short inertial range present for $8 < k < 20$ for the original scheme, however, at such low wave numbers there is only a small statistical sample, thus any power law dependence is masked by statistical fluctuations. There is a slight up-turning of the spectra at high wave numbers when using the modified method, indicating that the level of numerical dissipation is slightly lower than ideal for a sub-grid model for this application.

Such a large influence of the low Mach number correction on the high wave numbers is surprising. If it is assumed that the turbulent kinetic energy spectra conforms to a $k^{-3/2}$ form, then the characteristic velocity for a given wave number falls as $k^{-1/4}$. Assuming the peak of the spectrum is at $k = 4$, for $k = 100$ the mean

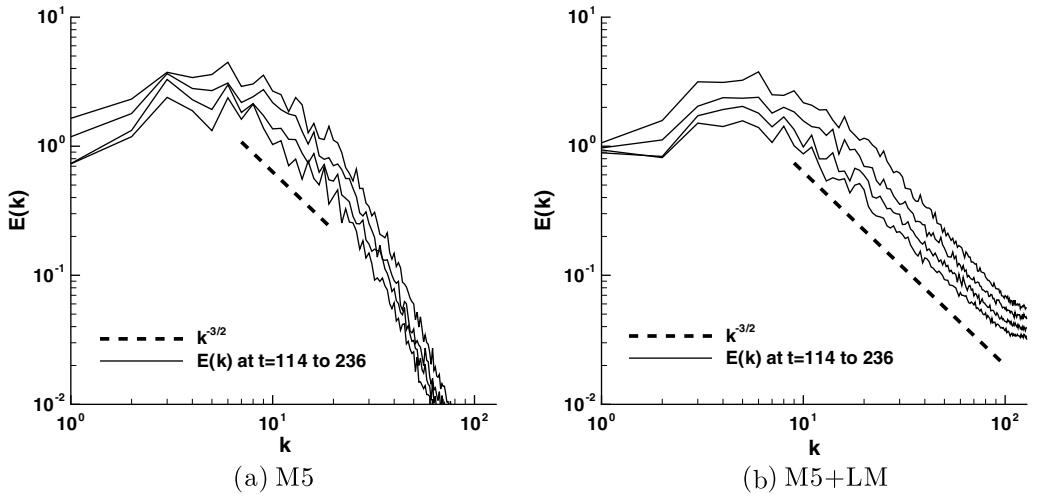

Fig. 16. Two-dimensional turbulent kinetic energy spectra taken at $t = 114, 154, 195$, and 236 plotted with a $k^{-3/2}$ line.

velocity would be approximately 0.4 of the peak velocity, which is not an excessively low Mach number in this test case ($M \approx 0.1$). Thus, the simulations have demonstrated that the seed instabilities resulting in such a spectrum are at a Mach number much less than the characteristic Mach number of the modes resolved on the grid assuming an inertial range form to the grid cut-off. These instabilities are damped at a very early stage in their growth by the original fifth-order method.

4. Conclusions

This paper has presented a simple modification of the finite volume Godunov method to significantly improve performance at low Mach number and in turbulent flows. It is shown analytically and through numerical test cases that the dissipation of the numerical scheme becomes constant in the limit of zero Mach number, as opposed to tending to infinity as is the case for the traditional scheme. In addition, this modification recovers the correct scaling of the pressure and density fluctuations as Mach number decreases. The key feature of the numerical scheme is that the reconstruction is modified *locally*, hence the scheme can capture both shock waves and low Mach number features in the same computational domain using the same formulation of the governing equations. The numerical modification adds negligible computational cost.

This paper has presented the results from applying such a modification to a standard Godunov-type method, however, in principle there is no reason why equivalent results would not be gained in a wider class of fully compressible schemes which rely on reconstruction of the conserved or primitive variables at the cell interface.

Acknowledgments

The authors would like to thank Anthony Weatherhead (AWE, Aldermaston) and Evgeniy Shapiro (Fluid Mechanics and Computational Science Group, Cranfield University) for their advice and suggestions whilst developing the methods, as well as Bill Rider (Sandia) for productive discussions. They would also like to acknowledge the financial support from EPSRC, MoD and AWE through the EPSRC(EP/C515153)-JGS (No. 971) project.

Appendix A. Mathematica script

This appendix details the Mathematica script used to computed the change in entropy over a single time step using van Leer extrapolation in a flow field where velocity varies, but pressure and density are locally constant.

```
(*Initial Conditions for interface i + 1/2 and soln of RP using the Taylor series
expansion of the van Leer limited velocities*)
pr = P[x];
pl = P[x];
ur = U[x] + dx U'[x]/2 + dx^2U''[x] - dx^4 U''''[x]/720 + dx^5 U''''[x]/60;
ul = U[x] + dx U'[x]/2 + dx^2U'' [x] - dx^4 U''''[x]/720 - dx^5 U''''[x]/60;
rr = R[x];
rl = R[x];
psp = (pr + pl)/2 + (ul - ur)(rr + rl) a/4;
usp = (ur + ul)/2 + (pl - pr)/((rr + rl) a);
rsp = rl + (ul - usp) (rr + rl)/2/a;


(*Initial Conditions for interface i - 1/2 and soln of RP using the Taylor series
expansion of the van Leer limited velocities*)
prm = P[x];
plm = P[x];
urm = U[x] - dx U'[x]/2 + dx^ 2U''[x] - dx^4 U''''[x]/720 + dx^5 U'''' [x]/60;
ulm = U[x] - dx U'[x]/2 + dx^ 2U''[x] - dx^4 U'''[x]/720 - dx^ 5 U''''[x]/60;
rrm = R[x];
rlm = R[x];
psm = (prm + plm)/2 + (ulm - urm)(rrm + rlm)a/4;
usm = (urm + ulm)/2 + (plm - prm)/((rrm + rlm) a);
rsm = rlm + (ulm - usm) (rrm + rlm)/2/a;


(*Compute conservative variables at the next time step*)
ul = R[x] + v (rsm usm - rsp usp);
u2 = R[x] U[x] + v (rsm usm^2 + psm - rsp usp^2 - psp);
u3 = P[x]/(g - 1) + R[x] U[x]^2/2 + v((psm g/(g - 1) + rsm usm^2/2)
usm - (psp g/(g - 1) + rsp usp^2/2)usp);


{*Calculate primitive variables at the next times step*)
rl = Simplify[Expand[ul]]
ul = Simplify[Expand[u2/ul]]
el = Simplify[Expand[u3]]
pl = (g - 1)(el - 1/2 rl ul^2)


(*Calculate the entropy change and multiply by temperature*)
ln = pl/rl^g ((rl)^g/(pl));
ds = RGAS/(g - 1)(ln - 1);
Tds = ds a^2/(g RGAS);


(*Substitute speed of sound instead of pressure p, and substitute dt for dx, CFL
and a*)
Tds2 = Tds/. p -> r a^2/g;
Tdsodt = Collect[Tds2/dt/. v -> dt/dx/. dt -> dx CFL/a, a];
```

To compute the entropy increase due to spatial discretisation, then it is necessary to repeat the above analysis for the exact Taylor series expansion of the cell average quantities to the cell interface, and then subtract

the entropy rise with the exact from the entropy rise of the M5 interpolated method. To analyse the modified scheme simply substitute in the following lines before computing the solution of the Riemann problem:

```
sum = (ur + ul)/2
diff = (ur - ul)sum/(2 a)
ur = sum + diff
ul = sum - diff
```

References

[1] B. Thornber, D. Drikakis, R. Williams, On entropy generation and dissipation of kinetic energy in high-resolution shock-capturing schemes, J. Comput. Phys. 227 (2008) 4853–4872.
[2] E. Toro, Riemann Solvers and Numerical Methods for Fluid Dynamics, Springer-Verlag, 1997.
[3] B. van Leer, Towards the ultimate conservative difference scheme.IV. A new approach to numerical convection, J. Comput. Phys. 23 (1977) 276–299.
[4] K. Kim, C. Kim, Accurate, efficient and monotonic numerical methods for multi-dimensional compressible flows part II: Multi-dimensional limiting process, J. Comput. Phys. 208 (2005) 570–615.
[5] H. Guillard, A. Murrone, On the behaviour of upwind schemes in the low Mach number limit: II. Godunov type schemes, Comput. Fluids 33 (2004) 655–675.
[6] B. Thornber, D. Drikakis, Numerical dissipation of upwind schemes in low Mach flow, Int. J. Numer. Meth. Fluids, 2007, doi:10.1002/fld.1628.
[7] P. Birken, A. Meister, Stability of preconditioned finite volume schemes at low Mach numbers, BIT 45 (2005) 463–480.
[8] R. Spiteri, S. Ruuth, A class of optimal high-order strong-stability preserving time discretization methods, SIAM J. Sci. Comput. 40 (2) (2002) 469–491.
[9] D. Drikakis, W. Rider, High-Resolution Methods for Incompressible and Low-Speed Flows, Springer Verlag, 2004.
[10] R. Klein, Semi-implicit extension of a Godunov-type scheme based on low Mach number asymptotics I: One-dimensional flow, J. Comput. Phys. 121 (1995) 213–237.
[11] W. Noh, Errors for calculations of strong shocks using and artificial viscosity and an artificial heat flux, J. Comput. Phys. 72 (1987) 78–120.
[12] R. Liska, B. Wendroff, Comparison of several difference schemes on 1D and 2D test problems for the Euler equations, SIAM J. Sci. Comput. 25 (3) (2003) 995–1017.
[13] S. Gottlieb, C.-W. Shu, Total variation diminishing Runge-Kutta schemes, Math. Comput. 67 (221) (1998) 73–85.
[14] D. Youngs, ILES of Rayleigh-Taylor and Richtmyer-Meshkov mixing, in: ECCOMAS 2006, 2006.
[15] H. Guillard, C. Viozat, On the behaviour of upwind schemes in the low Mach number limit, Comput. Fluids 28 (1999) 63–86.
[16] E. Garnier, M. Mossi, P. Sagaut, P. Comte, M. Deville, On the use of shock-capturing schemes for large-eddy simulation, J. Comput. Phys. 153 (1999) 273–311.
[17] B. Thornber, A. Mosedale, D. Drikakis, On the Implicit Large Eddy Simulation of homogeneous decaying turbulence, J. Comput. Phys. 226 (2007) 1902–1929.
[18] D. Youngs, Three-dimensional numerical simulation of turbulent mixing by Rayleigh-Taylor instability, Phys. Fluids A 3 (5) (1991) 1312–1320.
[19] D. Youngs, Application of MILES to Rayleigh-Taylor and Richtmyer-Meshkov mixing, AIAA-2003-4102.
[20] J. Hinze, Turbulence, 2nd edition., McGraw-Hill, 1975.
[21] P. Davidson, Turbulence – An Introduction for Scientists and Engineers, Oxford University Press, 2004.
[22] J. Domaradzki, Z. Xiao, P. Smolarkiewicz, Effective eddy viscosities in implicit large eddy simulations of turbulent flows, Phys. Fluids 15 (12) (2003) 3890–3893.
[23] J. Chollet, Two-point closures as a subgrid-scale modelling tool for large eddy simulations, in: Turbulent Shear Flows IV, Springer Verlag, 1984.
[24] R. Richtmyer, Taylor instability in shock acceleration of compressible fluids, Comm. Pure Appl. Math. 13 (1960) 297–319.
[25] E. Meshkov, Instability of the interface of two gases accelerated by a shock wave, Fluid Dyn. 43 (5) (1969) 101–104.
[26] D. Youngs, Effect of initial conditions on self-similar turbulent mixing, in: IWPCTM 9, 2004.
[27] R. Menikoff, Numerical anomalies mimicking physical effects, Tech. rep., Los Alamos, 1995.
[28] T. Clark, Y. Zhou, Growth rate exponents of Richtmyer-Meshkov mixing layers, J. Appl. Mech. 73 (2006) 268–461.
[29] Y. Zhou, A scaling analysis of turbulent flows driven by Rayleigh-Taylor and Richtmyer-Meshkov instabilities, Phys. Fluids 13 (2) (2001) 538–543.
[30] D. Youngs, Numerical simulation of mixing by Rayleigh-Taylor and Richtmyer-Meshkov instabilities, Laser Part. Beams 12 (1994) 725–750.

[31] B. Thornber, D. Youngs, D. Drikakis, High resolution methods for planar 3D Richtmyer-Meshkov instabilities, in: IWPCTM 10, 2006.
[32] R. Cohen, W. Dannevik, A. Dimits, D. Eliason, Y. Mirin, A.A. Zhou, D. Porter, P. Woodward, Three-dimensional simulation of a Richtmyer-Meshkov instability with a two-scale initial perturbation, Phys. Fluids 14 (10) (2002) 3692–3709.